Journal of Mechanics Engineering and Automation 12 (2022) 29-40
doi: 10.17265/2159-5275/2022.02.001

Full-Field Stress Analysis of Perforated Members from Aligned Single-Element Strain Gages

A. A. Khaja[1] and R. E. Rowlands[2]

1. Applied Materials, Inc., Santa Clara, CA 95138, USA

2. University of Wisconsin-Madison, Madison, WI 53706, USA

Abstract: Engineering members often include cutouts. Although the structural integrity of such members can be highly influenced by associated stresses, determining them may be very challenging for *finite* shapes operating in an industrial environment. This is particularly so if the loading is not well known, a common occurrence in practical situations. While photomechanical methods can be effective, they necessitate optical access to the component, something which is also often unavailable. Recognizing the above, this paper demonstrates ability to determine the complete stresses throughout a perforated tensile plate using only aligned, single-element strain gages rather than multi-element rosettes. Although reliability is verified using finite elements, an objective of the technique is for situations when finite element methods are not feasible, e.g., the loading is inadequately known. The approach is applicable to members fabricated from isotropic, orthotropic or functionally-graded materials and is not restricted to a particular shape, cutout arrangement or loading condition.

Key words: Structural integrity, stress analysis, strains, reliability.

Nomenclature

∇^4	Biharmonic operator
c_o, c_n, d_n	Airy coefficients
N	Terminating value of summation series
ϕ	Airy stress function
r	Radial coordinate
θ	Angle
E	Elastic modulus
R	Hole radius
F	Applied load
σ_o	Far-field stress
ε_o	Far-field strain
$[A]$	Airy matrix
$\{c\}$	Airy coefficient vector
$\{d\}$	Input data vector
$\{d'\}$	Predicted/reconstructed vector
C	Condition number
RMS	Root mean square
m	Number of input data values
k	Number of unknown airy coefficients
ε_{yy}	Cartesian strain component
σ_{rr},$\sigma_{\theta\theta}$,$\sigma_{r\theta}$	Polar stress components
σ_{xx},σ_{yy},σ_{xy}	Cartesian stress components

Corresponding author: R. E. Rowlands, Ph.D., emeritus professor, research field: experimental mechanics.

1. Introduction

Engineering members often involve complicated *finite* shapes which include holes and/or notches. The structural integrity of such members can be highly influenced by the associated stresses. However, theoretical stress analyses tend to be limited to *simple*, *infinite* geometries. Like numerical analyses, theoretical methods necessitate knowing the loading conditions. The latter are frequently unknown in practice. Acknowledging the above, the ability to obtain the complete stresses at and in the neighborhod of cutouts in engineering members from only discretely measured aligned uniaxial strains is developed. A finite tensile aluminum plate containing a central circular hole is an illustrative example (Fig. 1). The experimental-numerical-analytical hybrid approach processes the measured strains with an Airy stress function using least-squares. Strains are recorded with

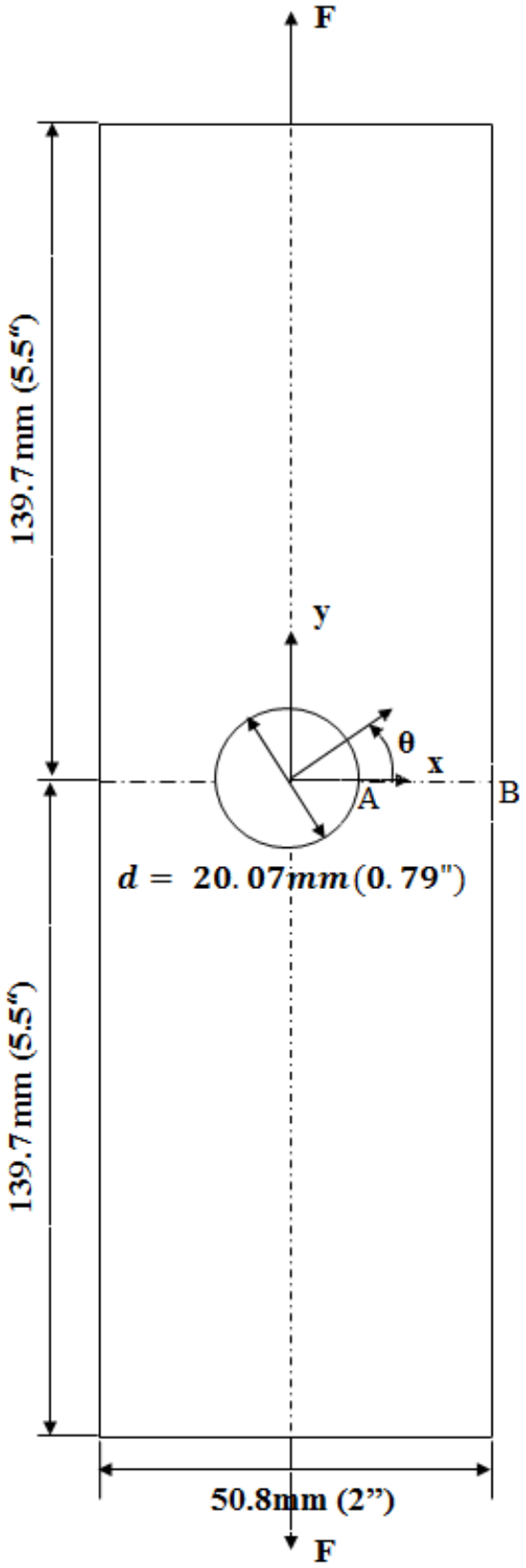

Fig. 1 Schematic diagram of perforate finite aluminum plate (6.35 mm thick).

commercial single-element metal foil strain gages and the traction-free conditions are satisfied analytically on the edge of the hole. Results are verified independently.

Extremely little literature is published on hybridizing measured strains with analytical and/or numerical tools. Ref. [1] analyzed a loaded perforated orthotropic composite by processing recorded strains using stress functions. The technique necessitated 2- and 3-element strain gage rosettes. In addition to being less expensive, the present ability to obtain all three components of stress from single-, rather than multi-element gages reduces the number of electronic channels needed. This simplifies the data acquisition requirements. Multi-element rosettes also pose the challenge that not all measured strains are at the same location. The question therefore arises at what common position does one assume the three strains occur. A pinned aluminum joint was stress analyzed by numerically processing recorded strains [2]. The strains were obtained from numerous extremely small commercial strip-gages. Bonding the strip-gages at different orientations provided the equivalence of multi-gage rosettes. Commercial strip gages having tiny elements are expensive and difficult to wire.

The authors are unaware of any published results of fully stress analyzing perforated or notched engineering members using aligned, single-element strain gages. Ref. [3] is relevent to the extent it stress analyzed a perforated member using a single component of optically recorded displacements. Unlike the present approach, photomechanical methods necessitate having optical access to the member. This is often unavailable in “real” situations. Furthermore, industrial organizations are more likely to have the equipment for, and experience with, strain gages than with optical methods such as moire, speckle, thermoelasticity or digital image correlation [4]. Optically recoded displacements also require differentiation to get strains and hence stresses, which is prone to errors.

The presented novel approach to stress analyze perforated or notched engineering members enables one to evaluate the structural integrity of optically inaccessible situations. The method is based on sound mechanics principles and has numerous advantages.

2. Relevant Stress and Strain Expressions

A relevant Airy stress function, ϕ, satisfying the biharmonic equation $\nabla^4\phi = 0$, equilibrium and compatibility for the geometry of Fig. 1 can be written as follows [5-7]:

$$\phi = a_0 + b_0 \ln r + c_0 r^2 + \sum_{n=2,4,6,..}^{N} \left\{\left(a_n r^n + b_n \mathrm{r}^{\mathrm{n}+2} + c_n r^{-n} + d_n \mathrm{r}^{-(\mathrm{n}-2)}\right)\cos n\theta\right\} \tag{1}$$

Imposing the traction-free condition on the boundary of the hole ($\sigma_{r\theta} = \sigma_{rr} = 0$ at $r = R$) for all values of θ gives the following stress and strain expressions [3].

$$\sigma_{rr} = \left(\frac{-2R^2}{r^2} + 2\right)c_0 - \sum_{n=2,4,...}^{\mathrm{N}} \left[\begin{Bmatrix} -(n-1)(n+1)R^2 r^{n-2} \\ +(n+1)R^{2(n+1)} r^{-(n+2)} \\ +(n+1)(n-2)r^n \end{Bmatrix} b_n + \begin{Bmatrix} -(n-1)R^{-2(n-1)} r^{n-2} \\ -(n-1)(n+1)R^2 r^{-(n+2)} \\ +(n-1)(n+2)r^{-n} \end{Bmatrix} d_n \right] cos(n\theta) \tag{2}$$

$$\sigma_{\theta\theta} = \left(\frac{2R^2}{r^2} + 2\right)c_0 + \sum_{n=2,4,...}^{N} \left[\begin{Bmatrix} -(n+1)(n-1)R^2 r^{n-2} \\ +(n+1)R^{2(n+1)} r^{-(n+2)} \\ +(n+1)(n+2)r^n \end{Bmatrix} b_n + \begin{Bmatrix} -(n-1)R^{-2(n-1)} r^{n-2} \\ -(n-1)(n+1)R^2 r^{-(n+2)} \\ +(n-1)(n-2)r^{-n} \end{Bmatrix} d_n \right] cos(n\theta) \tag{3}$$

$$\sigma_{r\theta} = \sum_{n=2,4,...}^{N} \left[\begin{Bmatrix} -(n+1)(n-1)R^2 r^{n-2} \\ -(n+1)R^{2(n+1)} r^{-(n+2)} \\ +n(n+1)r^n \end{Bmatrix} b_n + \begin{Bmatrix} -(n-1)R^{-2(n-1)} r^{n-2} \\ +(n-1)(n+1)R^2 r^{-(n+2)} \\ -n(n-1)r^{-n} \end{Bmatrix} d_n \right] sin(n\theta) \tag{4}$$

$$\sigma_{xx} = \left[\left\{-\cos 2\theta \frac{2R^2}{r^2} + 2\right\} c_0 + \sum_{n=2,4,...}^{N} \left\{ \begin{Bmatrix} (n+1)(n-1)R^2 r^{n-2}(\cos(n\theta - 2\theta)) \\ -(n+1)R^{2(n+1)} r^{-(n+2)}\left(cos(n\theta + 2\theta)\right) \\ -(n+1)r^n(n\cos(n\theta - 2\theta) - 2cosn\theta) \end{Bmatrix} b_n + \begin{Bmatrix} (n-1)R^{-2(n-1)} r^{n-2}(\cos(n\theta - 2\theta)) \\ +(n-1)(n+1)R^2 r^{-(n+2)}\left(cos(n\theta + 2\theta)\right) \\ -(n-1)r^{-n}(ncos(n\theta + 2\theta) + 2cosn\theta) \end{Bmatrix} d_n \right\} \right] \tag{5}$$

$$\sigma_{yy} = \left[\begin{array}{c} \left\{\cos 2\theta \frac{2R^2}{r^2} + 2\right\} c_0 \\ + \sum_{n=2,4,\ldots}^{N} \left\{ \begin{array}{c} \left\{ \begin{array}{c} -(n+1)(n-1)R^2 r^{n-2} \cos(n\theta - 2\theta) \\ +(n+1)R^{2(n+1)} r^{-(n+2)} cos(n\theta + 2\theta) \\ +(n+1)r^n (n\cos(n\theta - 2\theta) + 2cosn\theta) \end{array} \right\} b_n \\ + \left\{ \begin{array}{c} -(n-1)R^{-2(n-1)} r^{n-2} \cos(n\theta - 2\theta) \\ -(n-1)(n+)R^2 r^{-(n+2)} cos(n\theta + 2\theta) \\ +(n-1)r^{-n} (ncos(n\theta + 2\theta) - 2cosn\theta) \end{array} \right\} d_n \end{array} \right\} \end{array} \right] \quad (6)$$

$$\epsilon_{yy} = \frac{1}{\mathrm{E}} \left[\begin{array}{c} \left\{\cos 2\theta \frac{2R^2}{r^2}(1+\upsilon) + 2(1-\upsilon)\right\} c_0 \\ + \sum_{n=2,4,\ldots}^{N} \left\{ \begin{array}{c} \left\{ \begin{array}{c} -(n+1)(n-1)R^2 r^{n-2} \cos(n\theta - 2\theta)(1+\upsilon) \\ +(n+1)R^{2(n+1)} r^{-(n+2)} cos(n\theta + 2\theta)(1+\upsilon) \\ +(n+1)r^n (n\cos(n\theta - 2\theta)(1+\upsilon) + 2cosn\theta(1-\upsilon)) \end{array} \right\} b_n \\ + \left\{ \begin{array}{c} -(n-1)R^{-2(n-1)} r^{n-2} \cos(n\theta - 2\theta)(1+\upsilon) \\ -(n-1)(n+1)R^2 r^{-(n+2)} cos(n\theta + 2\theta)(1+\upsilon) \\ +(n-1)r^{-n} (ncos(n\theta + 2\theta)(1+\upsilon) - 2cosn\theta(1-\upsilon)) \end{array} \right\} d_n \end{array} \right\} \end{array} \right] \quad (7)$$

where r is the radial coordinate measured from the center of a hole, angle θ is measured counter-clockwise from the horizontal x-axis (Fig. 1), c_0, b_n, and d_n are Airy coefficients, E is the elastic modulus, v is Poisson's ratio and R is the hole radius. Eqs. (1)-(7) involve a summation over n, where n goes through positive even integers from 2 to N, and the total number of coefficients is given by $k = N + 1$.

3. Strain Gage Details and Plate Loading

The plate contains commercial strain gages mounted as indicated in Table 1, Fig. 2 and similarly on the back of the plate. Only single-element gages in the y-direction are used such that ϵ_{yy} is measured at numerous discrete locations and the Airy coefficients are determined from Eq. (7) and these measured values of ϵ_{yy}. Due to inadequate room to bond all gages in a single quadrant on one face of the plate, gages were mounted throughout the four quadrants on the front and back faces. Care was taken such that each gage has exclusive coordinates when shifted to the first quadrant.

Fifty-seven strain gages were bonded to the plate. Twelve (i.e., gages 21, 22, 24, 26, 29, 30, 32, 33, 34, 36, 37 and 38) out of the 57 gages malfunctioned, leaving 45 useful strain inputs (Table 1). Since all gages were mounted and the plate was tested at room temperature, no dummy gages were employed.

Table 1 lists the individual gage details and locations. Fig. 2 shows the strain-gaged region of the front face of the plate. The back face was similarly gaged. The x- and y-coordinates in Table 1 are to the center of the active portion of the gages. They are relative to an origin at the bottom right corner of the plate in Fig. 2. The numbers on the respective terminal tabs in Fig. 2 correspond to identification numbers of Table 1. Gage 57 of Table 1 was bonded on the transverse round boundary of the hole at $\theta = 0°$ in Fig. 2.

The instrumented plate was incrementally tested in a model 1000 universal Instron screw-driven testing machine (Fig. 3). Strains were recorded at several discrete increasing and decreasing load levels. Reported results are for F = 4,448.2 N (1,000 lbs); σ_o= 13.8 MPa (2,000 psi).

Table 1 Gage numbers, information and locations relative to lower-right hand corner of Fig. 2.

Gage number	Gage factor	Resistance (Ω)	*x* (mm)	*y* (mm)
1	2.070 ± 0.5%	120.1	2.39	137.31
2	2.070 ± 0.5%	120.0	6.76	137.31
3	2.070 ± 0.5%	120.0	11.13	137.31
4	2.070 ± 0.5%	120.1	36.12	130.18
5	2.070 ± 0.5%	119.8	40.49	130.18
6	2.070 ± 0.5%	119.9	45.24	130.18
7	2.060 ± 0.5%	119.8	1.60	147.65
8	2.060 ± 0.5%	119.9	5.56	147.65
9	2.060 ± 0.5%	119.8	10.31	147.65
10	2.060 ± 0.5%	119.9	37.31	139.70
11	2.060 ± 0.5%	1200	41.28	139.70
12	2.060 ± 0.5%	119.9	45.24	139.70
13	2.130 ± 0.5%	119.7	46.84	135.33
14	2.130 ± 0.5%	119.9	42.47	135.33
15	2.130 ± 0.5%	119.8	37.31	135.33
16	2.130 ± 0.5%	119.7	12.70	145.26
17	2.130 ± 0.5%	120..0	7.95	145.26
18	2.130 ± 0.5%	119.8	3.18	145.26
19	2.040 ± 1.0%	119.0	24.61	158.34
20	2.040 ± 1.0%	120.1	26.59	158.34
23	2.040 ± 1.0%	119.5	32.94	158.34
25	2.040 ± 1.0%	119.5	37.31	158.34
27	2.040 ± 1.0%	119.3	41.28	158.34
28	2.040 ± 1.0%	119.5	43.26	158.34
31	2.040 ± 1.0%	119.6	13.89	125.43
35	2.040 ± 1.0%	120.0	22.63	125.43
39	2.060 ± 0.5%	119.9	21.03	155.58
40	2.060 ± 0.5%	119.8	25.40	155.58
41	2.060 ± 0.5%	119.8	30.18	155.58
42	2.130 ± 0.5%	120.1	38.89	156.36
43	2.130 ± 0.5%	120.1	42.88	156.36
44	2.130 ± 0.5%	119.9	46.84	156.36
45	2.130 ± 0.5%	120.0	38.51	127.79
46	2.130 ± 0.5%	120.1	42.88	127.79
47	2.130 ± 0.5%	120.1	19.84	118.26
48	2.060 ± 0.5%	119.9	23.82	118.26
49	2.060 ± 0.5%	119,8	28.58	118.26
50	2.060 ± 0.5%	119.8	1.60	163.532
51	2.060 ± 0.5%	119.8	6.35	163.53
52	2.060 ± 0.5%	119.9	10.72	163.53
53	2.060 ± 0.5%	119.7	14.68	163.53
54	2.060 ± 0.5%	120.0	2.39	109.93
55	2.060 ± 0.5%	120.2	6.76	109.93
56	2.060 ± 0.5%	120.1	11.13	109.93
57	2.130 ± 0.5%	120.3	15.37	139.70

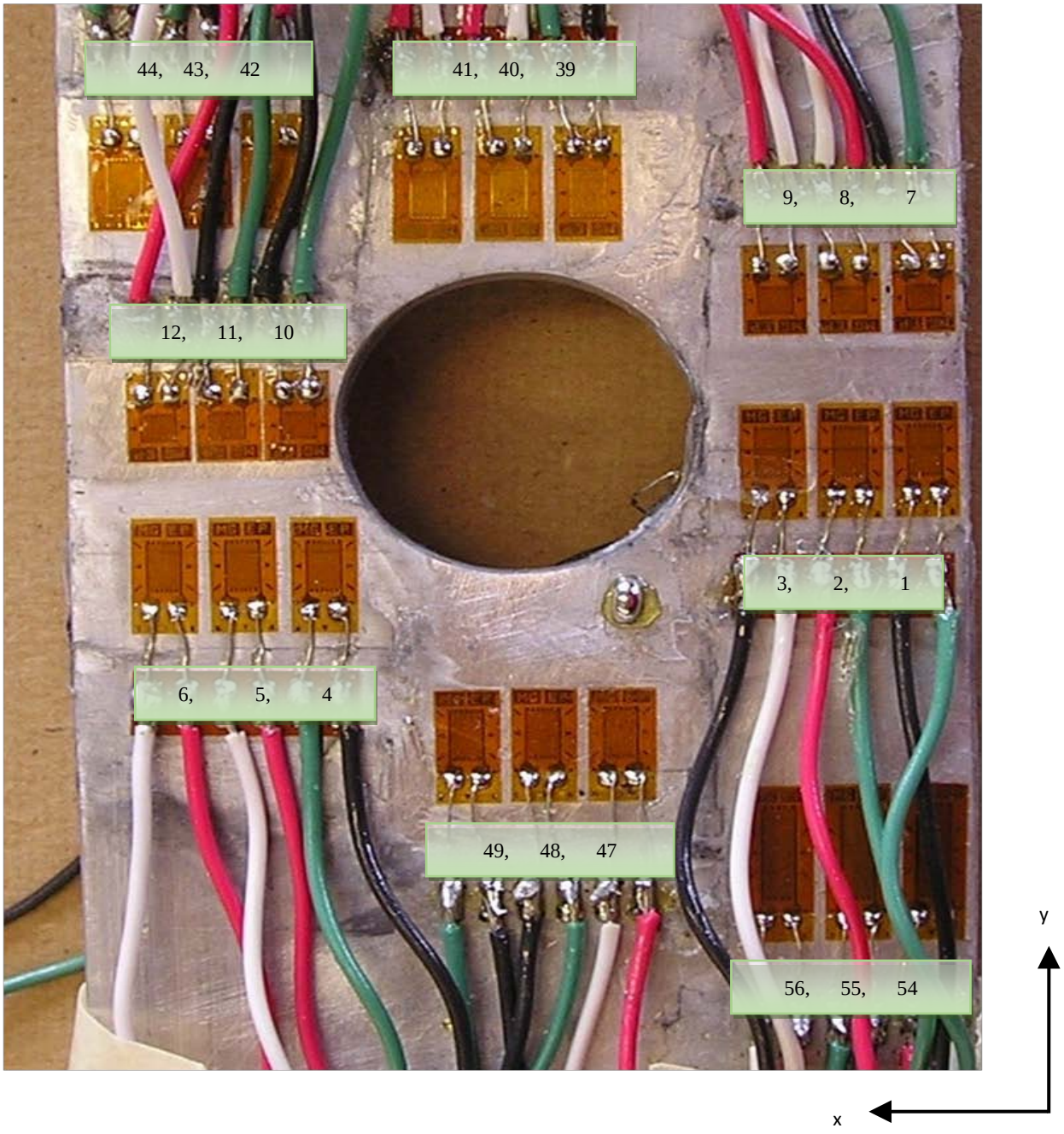

Fig. 2 Bonded strain gages showing gage numbers corresponding to Table 1 (front face).

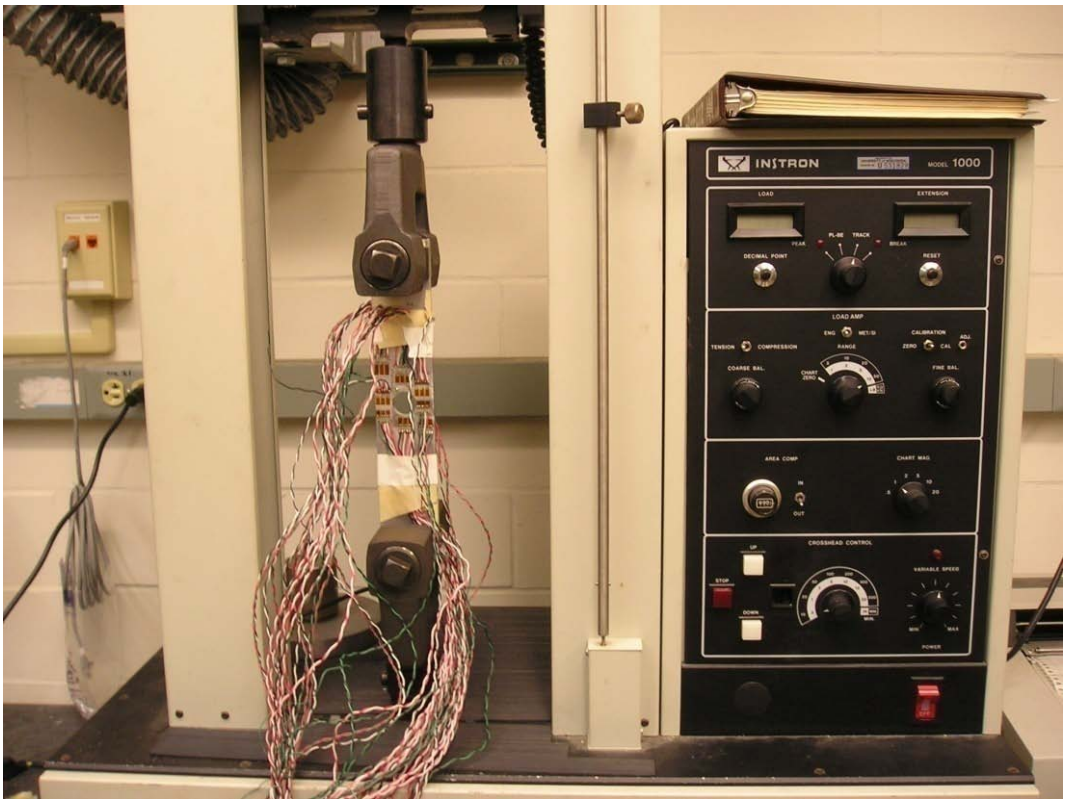

Fig. 3 Instrumented specimen being tested in Instron Machine.

4. Data Processing and Number of Coefficients

Since the plate is symmetrical about both *x*- and *y*-axes, all gage locations are identified in the first quadrant in Fig. 4 where the physical dimensions are normalized with respect to the radius of the hole.

Eq. (7) can be written in matrix form as Eq. (8) and the unknown Airy coefficients evaluated from the measured ε_{yy} strains from Eq. (9) using least squares. Item

$$\begin{bmatrix} \varepsilon_y(c_0, bn, dn) \\ \varepsilon_y(c_0, bn, dn) \\ \cdot \\ \cdot \\ \cdot \\ \cdot \\ \varepsilon_y(c_0, bn, dn) \end{bmatrix} \begin{bmatrix} c_0 \\ b_n \\ d_n \end{bmatrix} = \begin{bmatrix} \varepsilon_{y1} \\ \varepsilon_{y2} \\ \cdot \\ \cdot \\ \cdot \\ \varepsilon_{yN} \end{bmatrix} \tag{8}$$

or, in simplified form,

$$[A]_{m\times k}\{c\}_{k\times 1} = \{d\}_{m\times 1} \tag{9}$$

[*A*] is an *m* (number of input strains, i.e., *m* source locations in Fig. 4) by *k* (number of Airy coefficients) matrix containing a set of *m* linear strain equations involving *k* independent variables. Vector {*c*} contains the *k* unknown Airy coefficients, and vector {*d*} consists of the *m* measured strains corresponding to the strain equations in matrix [*A*]. Since there are more equations than unknowns, i.e., $m > k$, least-squares is utilized to solve the over-determined matrix expression $Ac = d$ of Eqs. (8) and (9). Knowing the values of the Airy coefficients (c_0, b_n, and d_n), the individual components of stress are available from Eqs. (2)-(6).

The root mean square, RMS, difference between the processed/reconstructed, {*d'*}, and recorded, {*d*}, strains, and the condition number, *C*, of matrix [*A*] were used to assess how many coefficients to retain (Figs. 5 and 6). The condition number, *C*, of matrix [*A*] measures the sensitivity of the solution of the system

of linear expressions of Eq. (8). It indicates the accuracy of the results from the matrix inversion and the linear equation solution. A low condition number is desired. Whereas Fig. 5 shows little change for at least $7 \leq k \leq 21$, the condition number results suggest $k \leq 7$ for reliable solutions. Results will be based on $k = 7$ and $N = 6$. However, Ref. [7] contains details which support also using $k = 13$.

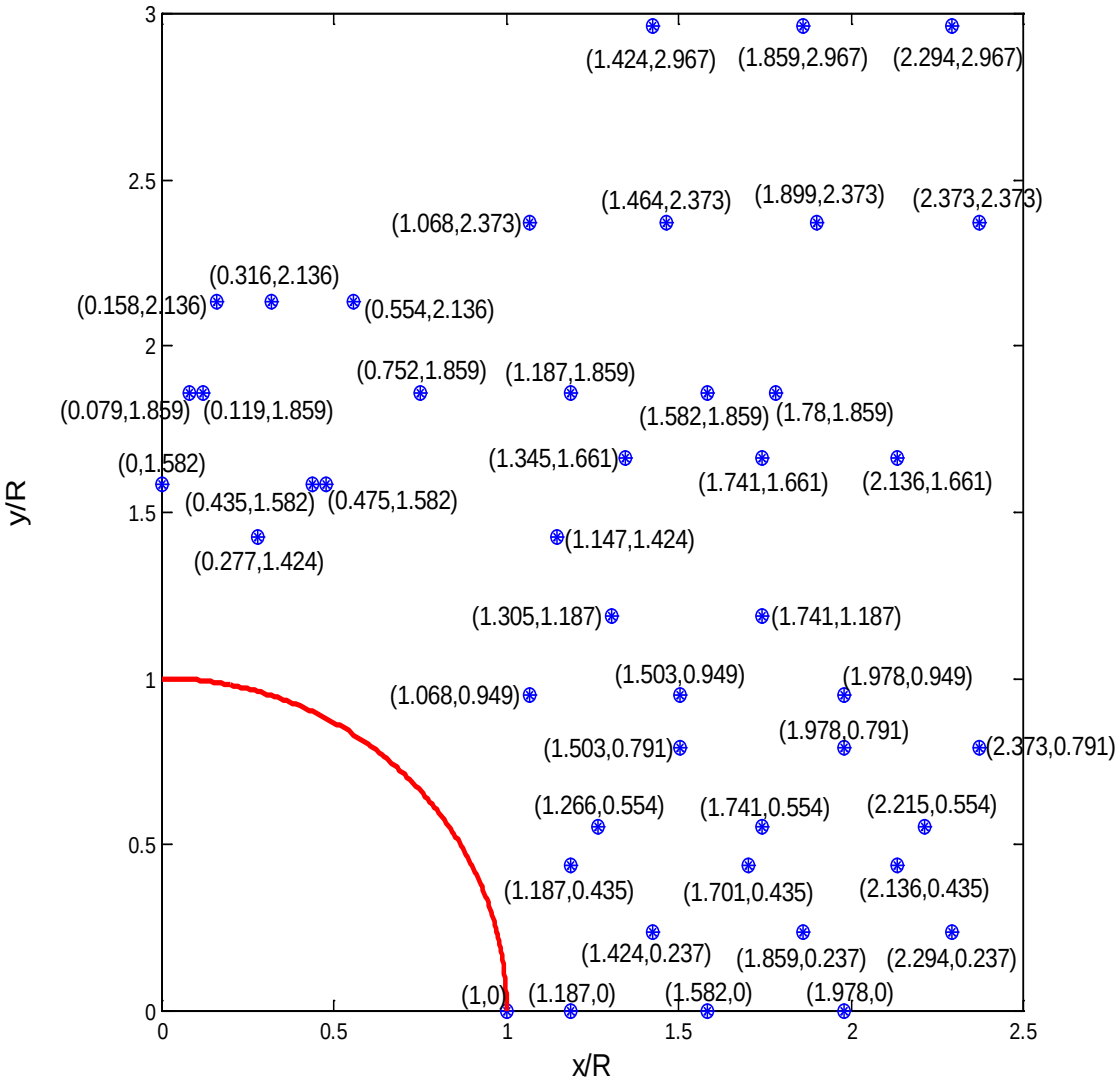

Fig. 4 Normalized gage coordinate locations of the 45 active gages.

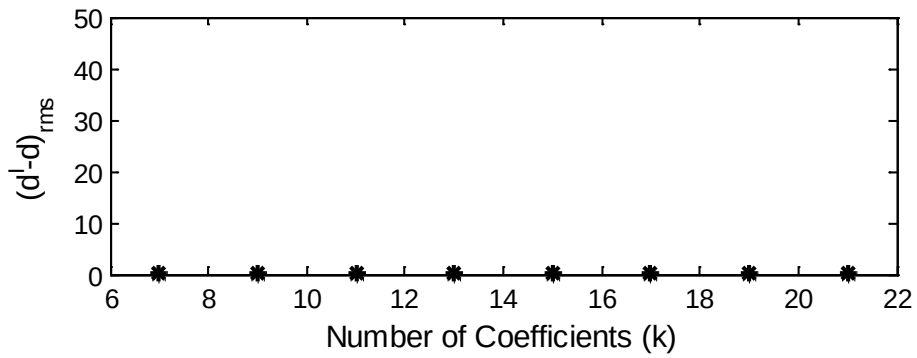

Fig. 5 Plot of RMS vs. number of coefficients, *k*, for *m* = 45 input values.

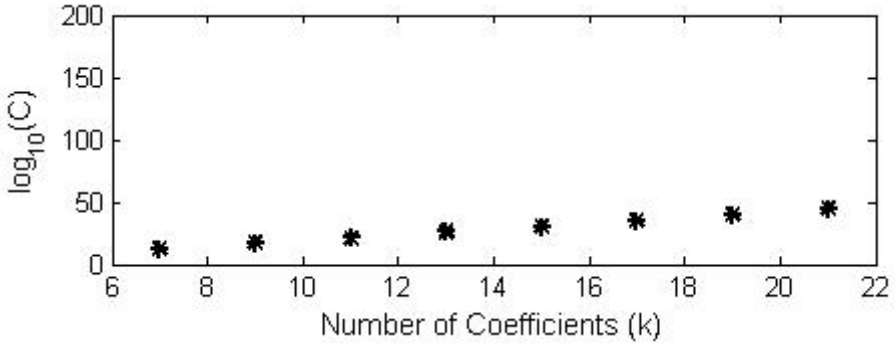

Fig. 6 Plot of $\log_{10}(C)$ vs. number of coefficients, k, for m = 45 input values.

5. FEA (Finite Element Analysis)

A FEA was conducted whose results will be compared with those from strain gages. Since the plate is symmetric about both x- and y-axes, a quarter-model was analyzed. Isoparametric elements (ANSYS element type: Plane-82) having 8 nodes per element were employed. The mesh was refined until the ANSYS results did not vary more than 0.1% on the periphery of hole. The final mesh covering the one quarter of the plate utilizes 6,700 elements and 20,473 nodes. A far field stress of 13.79 MPa = 2,000 psi was applied at the ends of the numerical model. Ref. [7] contains additional FEM details.

6. Results

Upon evaluating the Airy coefficients (c_0, b_n and d_n, for N = 6) from Eq. (9) and the measured strains, individual components of stress and strain were obtained from Eqs. (2)-(7). Results are based on all 45 gages as well as for just 41 gages (ignoring the input from gages 10 through 12 and 57 of Table 1 and Figs. 2 and 4). These results from the 45 gages are compared with those from FEA (ANSYS) and discrete strains (from gages 10, 11, 12 and 57) in Figs. 7-12 and Table 2. Measured strains are normalized with respect to the far field strain, ε_0 = 200 $\mu\varepsilon$ (based on the applied load, F = 4,448.2 N, gross area of 50.8 × 6.35 = 322.58 mm^2 and E = 69 GPa) and physical stresses are normalized by σ_o = 13.79 MPa.The physical dimensions associated with Figs. 9, 11 and 12 are plotted normalized with respect to the hole radius, R = 10.04 mm. Figs. 7 and 10 contain results on the edge of the hole, while Figs. 8, 9, 11 and 12 illustrate the situations away from the hole. The ability to provide stresses away from the hole can be important since the worst situation need not occur on the edge of holes or notches in orthotropic or functioning graded materials [8]. Results based on processing the recorded strains of the reliable 45 gages of Table 1 and Figs. 2 and 4 with the stress function agree well with those from FEM and the four discrete gages

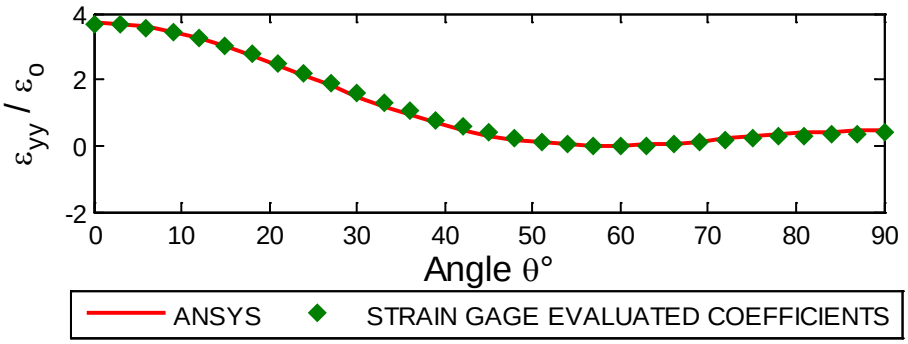

Fig. 7 Plot of $\varepsilon_{yy}/\varepsilon_0$ along boundary of hole from strain-gage evaluated Airy coefficients for k = 7 coefficients (m = 45 strain-gage input values) and ANSYS.

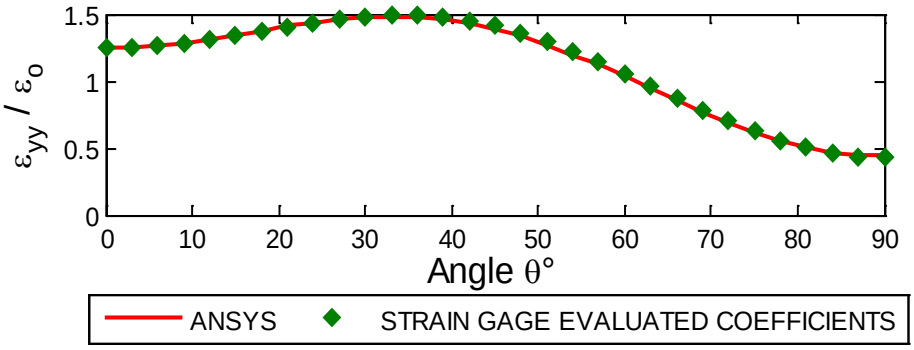

Fig. 8 Plot of $\varepsilon_{yy}/\varepsilon_0$ along r/R = 2 from strain-gage evaluated Airy coefficients for k = 7 coefficients (m = 45 strain-gage input values) and ANSYS.

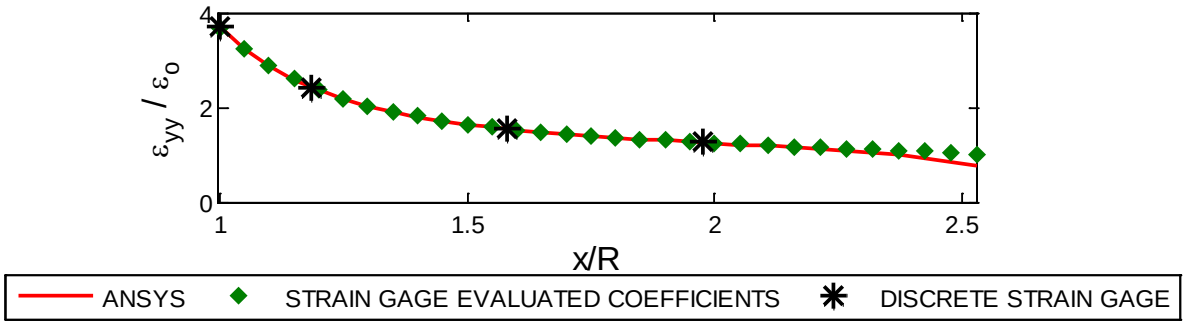

Fig. 9 Plot of $\varepsilon_{yy}/\varepsilon_0$ along AB of Fig. 1 from strain-gages (reconstructed using the evaluated Airy coefficients and discrete gages) for k = 7 coefficients (m = 45 strain-gage input values) and ANSYS.

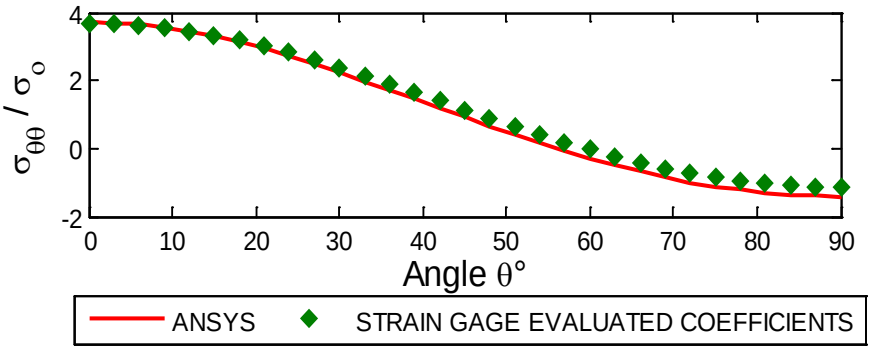

Fig. 10 Plot of $\sigma_{\theta\theta}/\sigma_0$ along boundary of hole from strain-gage evaluated Airy coefficients for k = 7 coefficients (m = 45 strain-gage input values) and ANSYS.

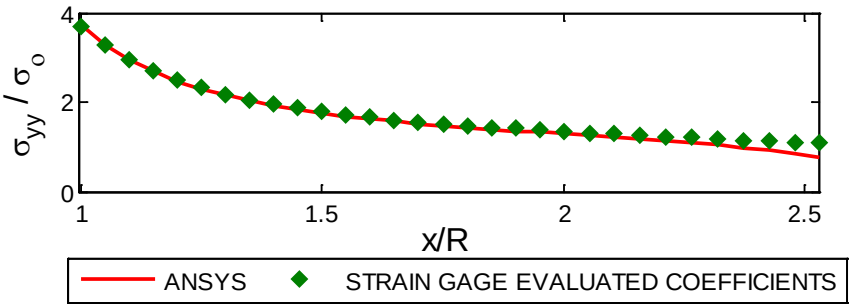

Fig. 11 Plot of σ_{yy}/σ_0 along AB of Fig. 1 from strain-gage evaluated Airy coefficients for k = 7 coefficients (m = 45 strain-gage input values) and ANSYS.

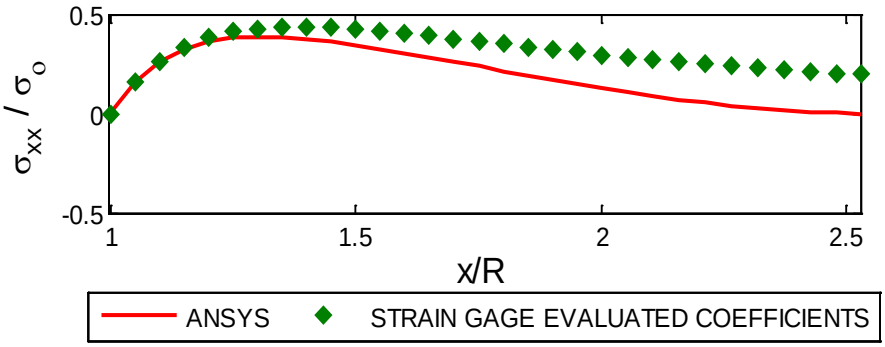

Fig. 12 Plot of σ_{xx}/σ_0 (= σ_{rr}/σ_0) along AB of Fig. 1 from strain-gage evaluated Airy coefficients for k = 7 coefficients (m = 45 strain-gage input values) and ANSYS.

Table 2 Normalized strains, $\varepsilon_{yy}/\varepsilon_0$ at discretely measured positions along line AB and those evaluated using the known Airy coefficients (m = 41).

		Normalized strains evaluated using Airy's stress function	
x/R	Individual strain gages	Number of coefficients, k = 7 and m = 41	Number of coefficients, k = 13 and m = 41
1.0	3.70	3.61	3.69
1.19	2.42	2.42	2.41
1.58	1.55	1.55	1.54
1.98	1.26	1.26	1.25

(gages 10 through 12 and 57) along line AB of Fig. 9. Although the ANSYS-predicted and strain-gage based stresses disagree along line AB in Fig. 12 for increasing x/R, these numbers are comparatively small.

7. Further Validation of Results

The results of Figs. 7-12 are based on the strains associated with the 45 gage locations of Fig. 4. As previously implied, this number of input values was subsequently reduced from 45 to 41 by omitting the four recorded strains (from gages 10 through 12 and 57) along line AB as input for evaluating the unknown Airy coefficients. Using the remaining 41 input values and k = 7 or 13, the normalized strains ($\varepsilon_{yy}/\varepsilon_0$) were evaluated [7]. Table 2 shows very good agreement between the discretely measured strains from the four individual gages (gages 10 through 12 and 57 of Fig. 2; i.e., $1.0 \le x/R \le 1.98$ in Table 2) and those computed at those four locations but based on strains recorded at the other 41 locations and processed using the Airy stress function. These results further validate the reliability of this hybrid technique.

8. Summary, Discussion and Conclusions

The paper's novelty is the demonstrated ability to determine the three independent components of stress at and throughout the neighborhood of a cutout in engineering members from only discretely measured *aligned uniaxial* strains. The latter were recorded with single-element strain gages and processed using an Airy stress function and least-squares. Rational methods were employed to assess how many Airy coefficients to retain. Reliable results are obtained using either 41 or 45 measured uniaxial strains and as few as seven Airy coefficients. However, results differ little whether one uses 7 or 13 Airy coefficients. Since the most important stresses in orthotropic composite or functionally graded materials need not occur at a hole or notch, results include those away from the edge of the hole.

The present approach benefits from using single-element strain gages. Although stacked rosettes circumvent the challenge that strains from different elements of a flat, multi-gage rosette does not occur at a common point, the upper elements of stacked rosettes

can provide incorrect data due to shear lag. The ability to avoid needing 2-or 3-element rosettes is particularly attractive if one wishes to use semiconductor or high-temperature strain gages. Such gages tend to be commercially prevalent only in single-element format. Thermally induced strains can occur in the gages if a gaged member operates at a temperature other than that at which the gages were applied. A common means of removing such strains is to employ dummy, as well as the active, strain gages. Being able to determine the complete stress fields using single-element gages rather than multi-element rosettes can greatly simplify the wiring, recording and data processing situations when employing dummy gages.

The present example fully stress analyzes the plate of Fig. 1 at and beyond the hole. In some cases the interest might be to obtain the stress only at the known location of the most serious situation on the edge of a cutout. This can be achieved sometimes by bonding a small strain gage on the transverse edge of the member at that position, e.g., like gage 57 of Table 1. However, this might not be feasible if the member is very thin or if the radius of curvature at the desired location is extremely small. Moreover, the location of the most serious stress on the edge of a cutout in an orthotropic composite material might not be known. The present ability to obtain stresses at re-entrant corners from strain gages well away from such geometric discontinuities overcomes such challenges.

Photomechanics can be effective for stress analyzing members. However, in addition to necessitating optical access to the member of interest, particularly industrial organizations are probably more likely to be better equipped and experienced using strain gages than optical methods.

The developed technology is demonstrated for a circular hole in a rectangular tensile aluminum plate but is applicable to more complicated geometries, orthotropic composites and even in-plane fatigue loading. Provided the loading is sufficiently slow to ignore dynamic effects, the method could potentially serve as an inspection tool by visually displaying a relevant plot such as the strain-gage results of Fig. 9 with time. The applied load could also be determined by integrating the longitudinal stress such as that of Fig. 11 across the width of the plate.

References

[1] Baek, T. H., and Rowlands, R. E. 2001. “Hybrid Stress Analysis of Perforated Composites using Strain Gages.” In *Experimental Mechanics* 41 (2): 195-203.

[2] Foust, B. E., and Rowlands, R. E. 2003. “Inverse Stress Analysis of Pinned Connections using Strain Gages and Airy Stress Function.” In *Inverse Problems in Engineering Mechanics (ISIP 2003)*, Nagano, Japan, M. Tanaka, 323-32.

[3] Khaja, A. A., Matthys, D. R., and Rowlands, R. E. 2014. “Determining all Displacements, Strains and Stresses Full-Field from Measured Values of a Single Displacement Component.” *Experimental Mechanics* 54 (3): 443-55.

[4] Shukla, A., and Dally, J. W. 2010. *Experimental Solid Mechanics*. Knoxville, Tennessee: College House Enterprises, LLC.

[5] Lin S. J. 2007. “Two- and Three-Dimensional Hybrid Photomechanical-Numerical Stress Analysis.” PhD thesis, University of Wisconsin-Madison.

[6] Soutas-Little, R. W. 1998. *Elasticity.* Mineola, New York: Dover Publications, Inc.

[7] Khaja, A. A. 2012. “Experimentally Determined Full-Field Stress, Strain and Displacements Analytically of Perforated Displacements in Finite Members.” Ph.D. thesis, University of Wisconsin-Madison.

[8] Konish, H. J., and Whitney, J. M. 1975. “Approximate Stresses in an Orthotropic Plate Containing a Circular Hole.” *Jour. Composite Materials* 9: 157-66.